

## Brightened emission of dark trions in transition-metal dichalcogenide monolayers

V. Jindal<sup>1\*</sup>, K. Mourzidis<sup>1\*</sup>, A. Balocchi<sup>1</sup>, C. Robert<sup>1</sup>, P. Li<sup>2</sup>, D. Van Tuan<sup>2</sup>, L. Lombez<sup>1</sup>, D. Lagarde<sup>1</sup>, P. Renucci<sup>1</sup>, T. Taniguchi<sup>3</sup>, K. Watanabe<sup>4</sup>, H. Dery<sup>2,5†</sup> and X. Marie<sup>1†</sup>

<sup>1</sup>*Université de Toulouse, INSA-CNRS-UPS, LPCNO, 135 Av. Rangueil, 31077 Toulouse, France*

<sup>2</sup>*Department of Electrical and Computer Engineering, University of Rochester, Rochester, New York 14627, USA*

<sup>3</sup>*International Center for Materials Nanoarchitectonics, National Institute for Materials Science, 1-1 Namiki, Tsukuba 305-00044, Japan*

<sup>4</sup>*Research Center for Functional Materials, National Institute for Materials Science, 1-1 Namiki, Tsukuba 305-00044, Japan*

<sup>5</sup>*Department of Physics and Astronomy, University of Rochester, Rochester, New York 14627, USA*

*The optical emission spectra of semiconducting transition-metal dichalcogenide monolayers highlight fascinating recombination processes of charged excitons (trions). When charge tunable WSe<sub>2</sub> monolayers are moderately doped with electrons, a strong luminescence peak emerges just below the well-understood spectral lines associated with the recombination of negatively charged bright and dark trions. Despite previous investigations, its origin remains elusive. Here, we demonstrate that this luminescence peak is the result of electron-electron assisted recombination that brightens the dark trion emission. Supporting evidence for this second-order recombination process comes from identifying the equivalent brightened emission of positively charged dark trions when the monolayer is electrostatically doped with holes. Remarkably, the discovered hole-hole assisted luminescence peak emerges in the near infrared, about 500 meV below the well-studied spectral region of excitons and trions. In addition to identifying new recombination channels of these excitonic complexes, our findings accurately determine the spin-split energies of the conduction and valence bands. Both of which play crucial roles in understanding the optical properties of WSe<sub>2</sub> based homo- and hetero-structures.*

\*These authors contributed equally to this work.

† [hdery@UR.Rochester.edu](mailto:hdery@UR.Rochester.edu) , [marie@insa-toulouse.fr](mailto:marie@insa-toulouse.fr)

The optical properties of atomically thin semiconductors based on transition-metal dichalcogenides (TMDs) are dominated by robust exciton complexes which give rise to rich physics associated with various interactions and correlation effects<sup>1-3</sup>. Charge-tunable WSe<sub>2</sub> monolayers are possibly the most studied model system due to their relatively high quality. When electrostatically doped with electrons, the luminescence spectra of the monolayer exhibit well identified peaks corresponding to the optical recombination of bright and dark negatively charged excitons (trions)<sup>4-7</sup>. Surprisingly, between slight and moderate densities of resident electrons, the most intense luminescence line does not correspond to these direct optical recombination channels: an intense luminescence component lying ~10 meV below the dark trion has been clearly identified by many groups in charge tunable WSe<sub>2</sub> monolayer devices<sup>4,8-11</sup>. Two fundamental questions arise: which exciton complex is associated with this optical recombination? And what is the nature of the recombination process? Several different interpretations were proposed. It was suggested that the line could result from the trion's fine structure<sup>4</sup>, the recombination of double charged trion X<sup>2-</sup>,<sup>9</sup> the coupling between excitons and short-range intervalley plasmons<sup>12</sup> or the consequence of the interaction between dark and bright trions<sup>13,14</sup>.

Here, we elucidate the origin of this luminescence line and demonstrate that its relatively intense emission is the result of a second-order transition that involves dark trions. A resonant effect associated with the electron-electron interaction yields radiative recombination along with spin-conserving intervalley transition of the left behind electron to the upper conduction band (the electron that originally resides in the same valley of the hole). As a result of energy conservation and translation symmetry, the emitted photon is shifted to lower energy compared to the dark trion by a value equal to the conduction band (CB) spin-orbit splitting  $\Delta_c$ . The interpretation is further strengthened by the fact that we observe and interpret the same type of second-order recombination channel for the positively charged trion when the monolayer is electrostatically doped with holes. It results in a near infrared emission line, as the emission is now downshifted by the valence band (VB) spin-orbit splitting  $\Delta_v$ , which is much larger than the CB one. These investigations yield accurate determinations of both CB and VB spin-orbit splitting energies. We find  $\Delta_c = 12.0 \pm 0.5$  meV and  $\Delta_v = 478 \pm 1$  meV. Previous experimental determinations of the valence band spin-orbit (SO) splitting were either based on Angle Resolved Photoemission Spectroscopy (ARPES) measurements with a spectral resolution of few tens of meV or reflectivity/transmission experiments which include contributions of both  $\Delta_c$  and  $\Delta_v$  as well as the binding energy of the exciton<sup>15,16</sup>.

## Results

We investigated high-quality charge tunable WSe<sub>2</sub> devices as sketched in Fig. 1a. Details on sample fabrication can be found in the Methods section<sup>17,18</sup>. A voltage bias applied between the monolayer and the back gate allows us to electrostatically dope the monolayer. The doping densities in either the electron- or hole-doped regimes are such that a change of 1 Volt in voltage bias corresponds to a typical change of  $0.8 \times 10^{11}$  cm<sup>-2</sup> in charge density<sup>19</sup>. We deliberately remain in the low-density regime to avoid collective phenomena, renormalization effects, and the emergence of hexcitons<sup>20</sup>. In this regime, the three-particle trion picture is an adequate description<sup>21,22</sup>. Continuous-wave polarization-dependent micro-photoluminescence (PL) experiments are performed in a closed cycle cryostat (T = 4 K), as explained in the Methods section.

**Brightened emission of the negatively charged dark trion.** Figure 1b displays the PL color plot as a function of bias voltage and photon energy. In the charge-neutral regime ( $V \sim -0.5$  volts), indicated by the horizontal dashed line, the recombination of bright (X<sup>0</sup>) and dark (D<sup>0</sup>) excitons dominate the PL spectrum<sup>23,24</sup>. When electrons are added to the monolayer (positive voltages), the PL intensity of the neutral exciton vanishes and we observe the well-known recombination of intravalley (singlet) X<sub>T</sub><sup>-</sup> and intervalley (triplet) X<sub>T</sub><sup>-</sup> negatively charged trions, composed of two electrons and one hole<sup>7,25</sup>. As shown in Fig. 2a,

the triplet trion is composed of a photogenerated electron-hole pair, made of an electron in the top CB and a missing electron in the topmost VB of the same  $K^+$  valley, and the pair is bound to a resident electron in the bottom CB of the time-reversed valley at  $K^-$ . For the singlet trion  $X_S^-$ , the three particles reside in the same valley, as shown in Fig. 2b. The emission of the dark trion ( $D^-$ ) is also detected at lower energy. As sketched in Fig. 2c,  $D^-$  is composed of two electrons in the lowest conduction bands at  $K^+$  and  $K^-$ , and a hole at the top of the valence band. Its radiative recombination for in-plane polarized light is forbidden. However it is allowed for z-polarized light<sup>10,11</sup>; the z-axis is perpendicular to the monolayer plane. The clear observation of  $D^-$  in the PL spectrum, as shown in Fig. 1, is the consequence of using high numerical aperture objective (NA=0.82) which allows us to detect the z-polarized luminescence component<sup>23</sup>. Importantly, we observe a bright line, labelled as  $D_B^-$ , lying 12 meV below  $D^-$ . This intense line was observed by many groups, but its origin remained unclear<sup>4,8,10,11</sup>. It was shown that this line is co-polarized with the laser, following circularly-polarized laser excitation and that its  $g$ -factor is about -4.5, *i.e.* close to the  $g$ -factor of bright trions or excitons<sup>24</sup>. In a work devoted to the general effects of exciton-electron and trion-electron interactions, it was first proposed that this transition could result from the brightened emission of the dark trion  $D^-$ <sup>26</sup>. The corresponding second-order recombination mechanism is summarized in Fig. 2d. The light is generated from recombination of the indirect exciton component composed of a conduction-band electron in  $K^-$  and a hole in  $K^+$ . To respect translation symmetry, the second electron of the trion ends-up in the opposite top valley (*i.e.*, Coulomb induced intervalley spin-conserving transition). As a result of energy conservation, the light emission is shifted to lower energy compared to the  $D^-$  transition by an amount equal to the conduction band spin-orbit splitting  $\Delta_c$ . The measured energy difference between  $D^-$  and  $D_B^-$  in Fig. 1(a) yields a direct measurement of the conduction band spin orbit splitting; we find  $\Delta_c \sim 12$  meV, in agreement with recent determinations<sup>19,27</sup>. As the  $D_B^-$  transition involves electronic transitions to the upper conduction band states, this explains that the associated  $g$ -factor is that of the bright trion (and not of the dark excitonic species)<sup>24</sup>. The schematics in Fig. 2d also illustrate why the emission of  $D_B^-$  is co-polarized with the laser following circularly polarized excitation, as observed experimentally<sup>14</sup>. We emphasize that contrary to the direct recombination process of bright or dark trions, the non-recombining electron in the dark trion is not merely a spectator during the  $D_B^-$  emission. Though this  $D_B^-$  emission results from a second-order process, its intensity is rather significant thanks to the resonance effect involving states in two nearby conduction bands. The interpretation of the  $D_B^-$  transition is strongly reinforced by the observation of an equivalent emission, linked to the same type of Coulomb induced second-order mechanism of positively charged trions.

**Brightened emission of the positively charged dark trion.** Figure 1b shows that in the hole-doped regime (negative voltages), the spectrum is dominated by the recombination of the bright positive trion  $X^+$  at 1.688 eV and the dark one  $D^+$  at 1.654 eV, as already observed by many groups<sup>8,9,28</sup>. Remarkably, when holes are injected in the monolayer, a new line shows up in the near-infrared region of the spectrum - beyond 1  $\mu\text{m}$  wavelength. Figure 3a displays the PL spectrum in this region, which clearly evidences a new line, labelled  $D_B^+$  at 1.175 eV; this line is absent in the neutral regime and its intensity rises with the voltage increase. Figure 3b shows that its intensity is commensurate with that of the dark trion  $D^+$ . This peak was not detected before, probably because its emission lies at much lower energies compared to those associated with other exciton species. The inset of Fig. 3b shows that the intensity of  $D_B^+$  rises with the excitation laser power, showing no sign of saturation, ruling out a possible interpretation based on impurity recombination. The energy difference between the resonances  $D_B^+$  and  $D^+$  is 478 meV (Fig. 3c). Notably, it is very close to the valence band spin-orbit splitting which has been calculated<sup>29</sup> and measured in ARPES ( $485 \pm 10$  meV)<sup>15</sup>. This is a strong argument to interpret the emission of  $D_B^+$  as the brightened emission of the dark trion  $D^+$ , following a second-order recombination mechanism like the one described above for the negatively charged dark trion  $D^-$ . The process is sketched in Fig. 3d, and it starts with a dark trion  $D^+$  comprising two holes in the  $K^+$  and  $K^-$  top valleys of the valence band and one electron at the bottom

of the conduction band. Owing to the hole-hole interaction, the  $D_B^+$  near-infrared recombination is facilitated by radiative recombination of the momentum-indirect electron-hole component of the trion. Energy and wavevector conservation rules are fulfilled thanks to the fact that the second hole ends up in the lower-energy valence band. As a consequence, the energy difference between the  $D^+$  and  $D_B^+$  lines can be used to extract the valence band spin-orbit splitting  $\Delta_v$ .

The interpretation of the  $D_B^+$  line is further confirmed by the measurement of the polarized luminescence following circularly polarized excitation.

The circularly polarized luminescence of  $D_B^+$  is measured following circularly polarized laser excitation with helicity  $\sigma^+$ . Figure 4a shows that the PL intensity counter-polarized with respect to the laser has a stronger intensity than the co-polarized PL component ( $I^{\sigma^+} < I^{\sigma^-}$ ). The resulted PL polarization degree is  $P_c = \frac{I^{\sigma^+} - I^{\sigma^-}}{I^{\sigma^+} + I^{\sigma^-}} \approx -0.25$ . This negative PL polarization can be well explained by the scenario summarized in Fig. 4b. The  $\sigma^+$  laser excitation yields the initial photogeneration of a bright positively charge trion  $X^+$  composed of an electron in the  $K^+$  valley of the upper conduction band and two holes in  $K^+$  and  $K^-$  valley respectively. The energy relaxation of the electron to the lowest CB leads to the formation of the dark trion  $D^+$ . This can occur through a spin conserving process implying inter-valley  $K_3$  phonon or an intra-valley relaxation based on  $\Gamma_5$  zone-center phonon<sup>24,30</sup>. As was shown in refs.<sup>18,24</sup>, the inter-valley process is dominant, meaning that the largest population of dark trions  $D^+$  following  $\sigma^+$  laser excitation has electrons lying in the  $K^-$  valley. Following hole-hole interaction, the second-order transition will yield a radiative recombination in the  $K^-$  valley, as shown in Fig. 4d. Consequently, a negative PL circular polarization of the  $D_B^+$  line is expected, as we observe experimentally.

## Discussion

The spectral positions of the brightened emission from dark trions and their polarization support the physical picture of charge-charge assisted recombination. One way to reassure this hypothesis is to compare the amplitudes of the emission lines  $D_B^-$  and  $D_B^+$ . By carefully taking into account the different detection efficiencies of both lines (spectrometer and detector response functions), the ratio between their integrated luminescence intensities is  $I_{D_B^-}/I_{D_B^+} \approx 70$  when the excitation laser power is 50  $\mu$ W, and the electrons or holes densities are  $3.6 \times 10^{11} \text{ cm}^{-2}$  corresponding to gate voltages of +4 V and -5 V respectively (the neutral regime corresponds to  $V \sim -0.5$  volts). This ratio can be compared with the calculated ratio between the brightened-emission recombination rates of negative ( $R^-$ ) and positive ( $R^+$ ) dark trions. Using second-order perturbation, the recombination rates ratio is

$$\frac{R^-}{R^+} = \frac{m_{c,t}}{m_{v,b}} \left| \frac{\Delta_v V_e}{\Delta_c V_h} \right|^2, \quad (1)$$

where  $m_{c,t}/m_{v,b}$  is the ratio between the effective masses of electrons in the top conduction band and holes in the bottom valence band, accounting for the density of states in the valleys of the left-behind charge particles.  $V_{e(h)}$  is the matrix element denoting the electron-electron (hole-hole) intervalley Coulomb interaction. Note that the ratio excludes the dipole-transition matrix element because the emission process involves recombination of similar electron and hole states in either positive or negative dark trions. Employing the calculated first-principal values of effective masses  $m_{c,t} = 0.29$  and  $m_{v,b} = 0.54$ <sup>29</sup>, and the measured SO energy splittings,  $\Delta_v = 478 \text{ meV}$  and  $\Delta_c = 12 \text{ meV}$ , the calculated ratio  $R^-/R^+ \sim 850 \cdot (V_e/V_h)^2$ . We can think of two possible ways to reconcile this result with the measured value  $I_{D_B^-}/I_{D_B^+} \approx 70$ . The first one is that central-cell corrections of the shortwave Coulomb interaction render the hole-hole matrix element stronger, such that  $V_h \sim 3.5V_e$ . While detailed calculations of central-cell corrections are beyond the scope of this paper, we notice that this behavior is reminiscent of the ratio between the zone-

edge phonon replica emissions of dark trions<sup>24,26</sup>. In more detail, similar to the intensity ratio between  $I_{D_B^-}$  and  $I_{D_B^+}$ , the emission amplitude of the  $K_1$  phonon replica is also not three orders of magnitude smaller than that of the  $K_3$  phonon replica, indicative of a stronger intervalley transition in the valence band (assisted by the  $K_1$  mode) compared with the conduction band (assisted by the  $K_3$  mode). The second possible reason to reconcile the measured and calculated ratios,  $I_{D_B^-}/I_{D_B^+}$  versus  $R^-/R^+$ , is that the bottom valence-band valleys at  $\pm K$  are nearly degenerate with the valence band valley at  $\Gamma$ , as suggested by recent ARPES experiments<sup>15,16,31</sup>. The intervalley transition from the top valley of  $K$  to the valley at  $\Gamma$  respects the same translation symmetry conditions, implying that their contributions should be added if these valleys are indeed energy degenerate. The experimental result can then be explained by the much larger effective mass (and ensuing density of states) of the  $\Gamma$  valley.

Another difference between the emission lines  $D_B^-$  and  $D_B^+$  is that the linewidth of  $D_B^+$  is about ten times larger than that of  $D_B^-$  (Fig. 3c). The measured full width at half maximum of  $D_B^+$  is  $\sim 24$  meV, showing no dependence on the holes density in the studied range between 0 and  $\sim 5 \cdot 10^{11} \text{ cm}^{-2}$ . We attribute the large broadening to the ultrafast lifetime of the free hole in the bottom valence band (Fig. 3d). The ultrafast lifetime could stem from efficient intervalley hole scattering between the nearly degenerate valence band valley at  $\Gamma$  and the valleys at  $\pm K$ <sup>15,16,31</sup>. Such efficient scattering has no parallel in the conduction band. Similarly, spin-conserving intervalley transition mediated by  $K_1$  phonon can lead to ultrafast transition of the hole from the bottom valley to the top opposite valley, whereas equivalent transition with  $K_3$  mode in the conduction band is hampered by phonon bottleneck ( $\Delta_c > E_{K_3}$ ). All in all, the strikingly different linewidths of  $D_B^-$  and  $D_B^+$  can be reasoned by a relatively long lifetime of a free electron in the top conduction band compared with that of a free hole in the bottom valence band.

Finally, the accurate determination of SO splitting energy in both conduction and valence bands provides valuable information on the difference between binding energies of A and B neutral excitons. The A exciton has been investigated in great detail both experimentally and theoretically in WSe<sub>2</sub> monolayer<sup>2,32</sup>. However, less is known about the B exciton which comprises an electron in the bottom conduction band and a hole in the bottom valence band (whereas the A exciton comprises an electron in the top conduction band and hole in the top valence band). The photon energy that resonates with the A(B) exciton can be written as  $E^{A(B)} = E_g + \Delta_{c(v)} - E_b^{A(B)}$ , where  $E_g$  is the free carrier gap involving the bands edges (bottom conduction band and top valence band), and  $E_b^{A(B)}$  is the binding energy of A(B) exciton. Thus, the energy difference between B and A excitons, measured in reflectivity or transmission experiments is

$$E^B - E^A = \Delta_v - \Delta_c - (E_b^B - E_b^A). \quad (2)$$

Though measurements of  $E^B - E^A$  have been commonly used to roughly estimate the valence band SO splitting  $\Delta_v$ <sup>2,6,33</sup>, Eq. (2) highlights that it also depends on the small SO splitting in the conduction band. For hBN encapsulated WSe<sub>2</sub> monolayer, differential reflectivity experiments yield  $E^B - E^A = 430 \text{ meV}$ <sup>34</sup>. This energy difference is clearly smaller than the valence band SO splitting  $\Delta_v \sim 478 \text{ meV}$ , which can be determined independently from the measured energy difference between the resonances  $D^+$  and  $D_B^+$  in the PL spectrum. Using  $\Delta_v$  and  $\Delta_c$  measured here, we find that  $E_b^B - E_b^A \approx 36 \text{ meV}$ . The larger binding energy of the B exciton can be attributed to the larger effective masses of its electron and hole components<sup>35</sup>. Indeed, if we use k.p theory to evaluate the effective masses in the corresponding valleys, the masses are typically smaller than that of the electron mass in vacuum ( $m_0$ ) by a factor that is commensurate with  $p^2/E_g$ , where  $p$  and  $E_g$  are the in-plane dipole transition and energy gap between the corresponding conduction and valence states. The effective masses of the electron and hole of the A exciton are expected to be smaller because of the smaller energy gap in this case. Using the calculated effective masses from density-functional theory, the masses of the electron and hole components of the A exciton are  $0.29m_0$  and  $0.36m_0$ ,

respectively, and those of the B exciton are  $0.4m_0$  and  $0.54m_0$ <sup>29</sup>. The resulting reduced masses of the A and B excitons are  $0.16m_0$  and  $0.23m_0$ , thereby supporting the larger binding energy of the B exciton.

**Acknowledgements** : This work was supported by the Agence Nationale de la Recherche under the program ESR/EquipEx+ (Grant No. ANR-21-ESRE- 0025) and ANR projects ATOEMS, IXTASE and PEPR SPIN. Work at the University of Rochester was supported by the DOE Basic Energy Sciences, Division of Materials Sciences and Engineering, under Award No. DE-SC0014349.

## Methods

**Sample fabrication.** We have fabricated a van der Waals heterostructure made of an exfoliated ML-WSe<sub>2</sub> embedded in high quality hBN crystals using a dry stamping technique in the inert atmosphere of a glove box<sup>36,37</sup>. The layers are deterministically transferred on top of a SiO<sub>2</sub>/Si substrate with Ti/Au electrodes patterned by photolithography. Flux-grown WSe<sub>2</sub> bulk crystals are purchased from 2D semiconductors. We use few layers of graphene exfoliated from a Highly Ordered Pyrolytic Graphite (HOPG) bulk crystal for the back gate and to contact the ML-WSe<sub>2</sub>.

**Experimental set-up.** Low temperature photoluminescence measurements were performed in a home built micro-spectroscopy set-up built around a closed-cycle, low vibration cryostat (T=4 K). The sample is excited by a He-Ne laser (632.8 nm). The PL signal is dispersed by a monochromator and detected by a silicon based charged-coupled device camera<sup>38</sup>. Unless otherwise stated, the excitation power is typically ~50  $\mu$ W, focused to a spot size of ~1  $\mu$ m diameter.

## References

1. Xu, X., Yao, W., Xiao, D. & Heinz, T. F. Spin and pseudospins in layered transition metal dichalcogenides. *Nature Phys* **10**, 343–350 (2014).
2. Wang, G. *et al.* Colloquium: Excitons in atomically thin transition metal dichalcogenides. *Rev. Mod. Phys.* **90**, 021001 (2018).
3. Mak, K. F. & Shan, J. Semiconductor moiré materials. *Nat. Nanotechnol.* **17**, 686–695 (2022).
4. Jones, A. M. *et al.* Optical generation of excitonic valley coherence in monolayer WSe<sub>2</sub>. *Nature Nanotech* **8**, 634–638 (2013).
5. Mak, K. F. *et al.* Tightly bound trions in monolayer MoS<sub>2</sub>. *Nature Mater* **12**, 207–211 (2013).
6. Wang, G. *et al.* Valley dynamics probed through charged and neutral exciton emission in monolayer WSe<sub>2</sub>. *Phys. Rev. B* **90**, 075413 (2014).
7. Courtade, E. *et al.* Charged excitons in monolayer  $\{\mathrm{WSe}\}_2$ : Experiment and theory. *Phys. Rev. B* **96**, 085302 (2017).
8. Ye, Z. *et al.* Efficient generation of neutral and charged biexcitons in encapsulated WSe<sub>2</sub> monolayers. *Nat Commun* **9**, 3718 (2018).
9. Barbone, M. *et al.* Charge-tunable biexciton complexes in monolayer WSe<sub>2</sub>. *Nat Commun* **9**, 3721 (2018).
10. Liu, E. *et al.* Gate Tunable Dark Trions in Monolayer WSe<sub>2</sub>. *Phys. Rev. Lett.* **123**, 027401 (2019).
11. Li, Z. *et al.* Direct Observation of Gate-Tunable Dark Trions in Monolayer WSe<sub>2</sub>. *Nano Lett.* **19**, 6886–6893 (2019).
12. Van Tuan, D., Scharf, B., Žutić, I. & Dery, H. Marrying Excitons and Plasmons in Monolayer Transition-Metal Dichalcogenides. *Phys. Rev. X* **7**, 041040 (2017).
13. Danovich, M., Zólyomi, V. & Fal’ko, V. I. Dark trions and biexcitons in WS<sub>2</sub> and WSe<sub>2</sub> made bright by e-e scattering. *Sci Rep* **7**, 45998 (2017).
14. Tu, J.-S., Borghardt, S., Grützmacher, D. & Kardynał, B. E. Experimental observation of a negative grey trion in an electron-rich WSe<sub>2</sub> monolayer. *J. Phys.: Condens. Matter* **31**, 415701 (2019).
15. Nguyen, P. V. *et al.* Visualizing electrostatic gating effects in two-dimensional heterostructures. *Nature* **572**, 220–223 (2019).
16. Zribi, J. *et al.* Strong interlayer hybridization in the aligned SnS<sub>2</sub>/WSe<sub>2</sub> hetero-bilayer structure. *npj 2D Mater Appl* **3**, 27 (2019).
17. Robert, C. *et al.* Measurement of Conduction and Valence Bands g-Factors in a Transition Metal Dichalcogenide Monolayer. *Phys. Rev. Lett.* **126**, 067403 (2021).
18. Robert, C. *et al.* Spin/valley pumping of resident electrons in WSe<sub>2</sub> and WS<sub>2</sub> monolayers. *Nat Commun* **12**, 5455 (2021).
19. Ren, L. *et al.* Measurement of the conduction band spin-orbit splitting in WSe<sub>2</sub> and WS<sub>2</sub> monolayers. *Phys. Rev. B* **107**, 245407 (2023).
20. Van Tuan, D., Shi, S.-F., Xu, X., Crooker, S. A. & Dery, H. Hexcitons and oxcitons in monolayer WSe<sub>2</sub>. *Phys. Rev. Lett.* **129**, 076801 (2022).
21. Sidler, M. *et al.* Fermi polaron-polaritons in charge-tunable atomically thin semiconductors. *Nature Phys* **13**, 255–261 (2017).

22. Glazov, M. M. Optical properties of charged excitons in two-dimensional semiconductors. *J. Chem. Phys.* **153**, 034703 (2020).
23. Wang, G. *et al.* In-Plane Propagation of Light in Transition Metal Dichalcogenide Monolayers: Optical Selection Rules. *Phys. Rev. Lett.* **119**, 047401 (2017).
24. He, M. *et al.* Valley phonons and exciton complexes in a monolayer semiconductor. *Nat Commun* **11**, 618 (2020).
25. Jones, A. M. *et al.* Excitonic luminescence upconversion in a two-dimensional semiconductor. *Nature Phys* **12**, 323–327 (2016).
26. Yang, M. *et al.* Relaxation and darkening of excitonic complexes in electrostatically doped monolayer WSe<sub>2</sub>: Roles of exciton-electron and trion-electron interactions. *Phys. Rev. B* **105**, 085302 (2022).
27. Kapuściński, P. *et al.* Rydberg series of dark excitons and the conduction band spin-orbit splitting in monolayer WSe<sub>2</sub>. *Commun Phys* **4**, 186 (2021).
28. Wang, Z., Shan, J. & Mak, K. F. Valley- and spin-polarized Landau levels in monolayer WSe<sub>2</sub>. *Nature Nanotech* **12**, 144–149 (2017).
29. Kormányos, A. *et al.*  $\mathbf{k} \cdot \mathbf{p}$  theory for two-dimensional transition metal dichalcogenide semiconductors. *2D Mater.* **2**, 022001 (2015).
30. Song, Y. & Dery, H. Transport Theory of Monolayer Transition-Metal Dichalcogenides through Symmetry. *Phys. Rev. Lett.* **111**, 026601 (2013).
31. Yeh, P.-C. *et al.* Layer-dependent electronic structure of an atomically heavy two-dimensional dichalcogenide. *Phys. Rev. B* **91**, 041407 (2015).
32. Zipfel, J. *et al.* Spatial extent of the excited exciton states in WS<sub>2</sub> monolayers from diamagnetic shifts. *Phys. Rev. B* **98**, 075438 (2018).
33. Koperski, M. *et al.* Optical properties of atomically thin transition metal dichalcogenides: observations and puzzles. *Nanophotonics* **6**, 1289–1308 (2017).
34. Manca, M. *et al.* Enabling valley selective exciton scattering in monolayer WSe<sub>2</sub> through upconversion. *Nat Commun* **8**, 14927 (2017).
35. Stier, A. V., McCreary, K. M., Jonker, B. T., Kono, J. & Crooker, S. A. Exciton diamagnetic shifts and valley Zeeman effects in monolayer WS<sub>2</sub> and MoS<sub>2</sub> to 65 Tesla. *Nat Commun* **7**, 10643 (2016).
36. Castellanos-Gomez, A. *et al.* Deterministic transfer of two-dimensional materials by all-dry viscoelastic stamping. *2D Mater.* **1**, 011002 (2014).
37. Cadiz, F. *et al.* Excitonic Linewidth Approaching the Homogeneous Limit in MoS<sub>2</sub> - Based van der Waals Heterostructures. *Phys. Rev. X* **7**, 021026 (2017).
38. Shree, S., Paradisanos, I., Marie, X., Robert, C. & Urbaszek, B. Guide to optical spectroscopy of layered semiconductors. *Nat Rev Phys* **3**, 39–54 (2020).

Figures

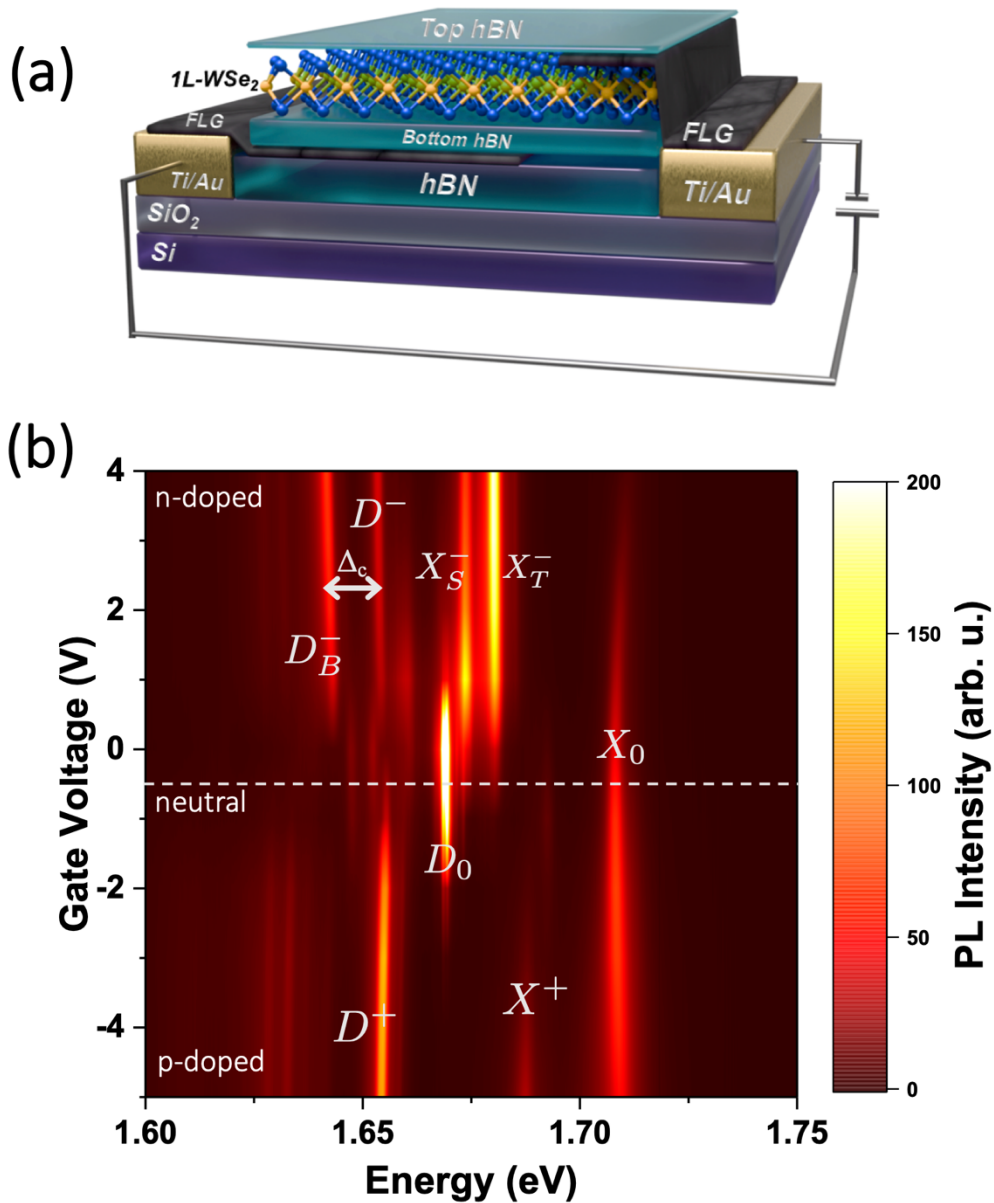


**Fig.1 Photoluminescence as a function of the gate voltage.** **a** Sketch of the charge adjustable WSe<sub>2</sub> monolayer device. **b** Photoluminescence intensity as a function of the gate voltage displaying the recombination of the different exciton complexes; the excitation energy is 1.96 eV. The brightened negatively charged exciton resulting from a second-order recombination process is labelled  $D_B^-$ .

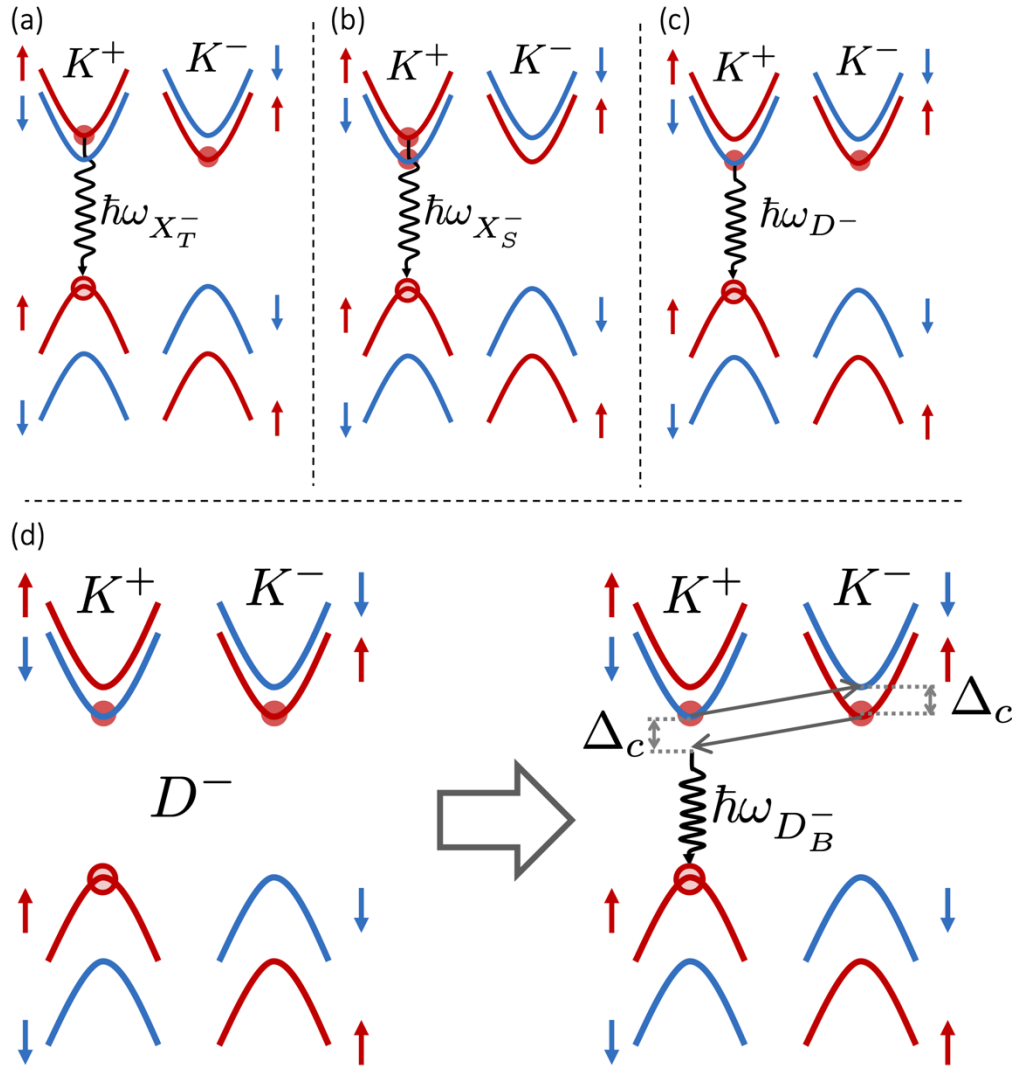


**Fig. 2 Negatively charged exciton recombination channels.** **a** and **b** Schematic of the bright triplet ( $X_T^-$ ) and singlet ( $X_S^-$ ) trion emission. **c** sketch of the dark ( $D^-$ ) trion radiative recombination which is z-polarized. **d** Illustration of the second order transition starting from the dark trion ( $D^-$ ) and yielding the radiative emission of the brightened dark trion ( $D_B^-$ ) line : the light is generated from recombination of the indirect exciton component composed of the conduction band electron in K<sup>-</sup> and and hole in K<sup>+</sup> valley. As a result of energy and wavevector conservation, the second electron of the trion ends-up in the opposite top valley (Coulomb induced inter-valley spin-conserving transition) and the process yields a light emission shifted to lower energy compared to the  $D^-$  transition by an amount equal to the conduction band spin-orbit splitting  $\Delta_c$ . In contrast to the direct optical recombination of bright or dark trion (as in **a**, **b** or **c**), the second electron here is no more a spectator.

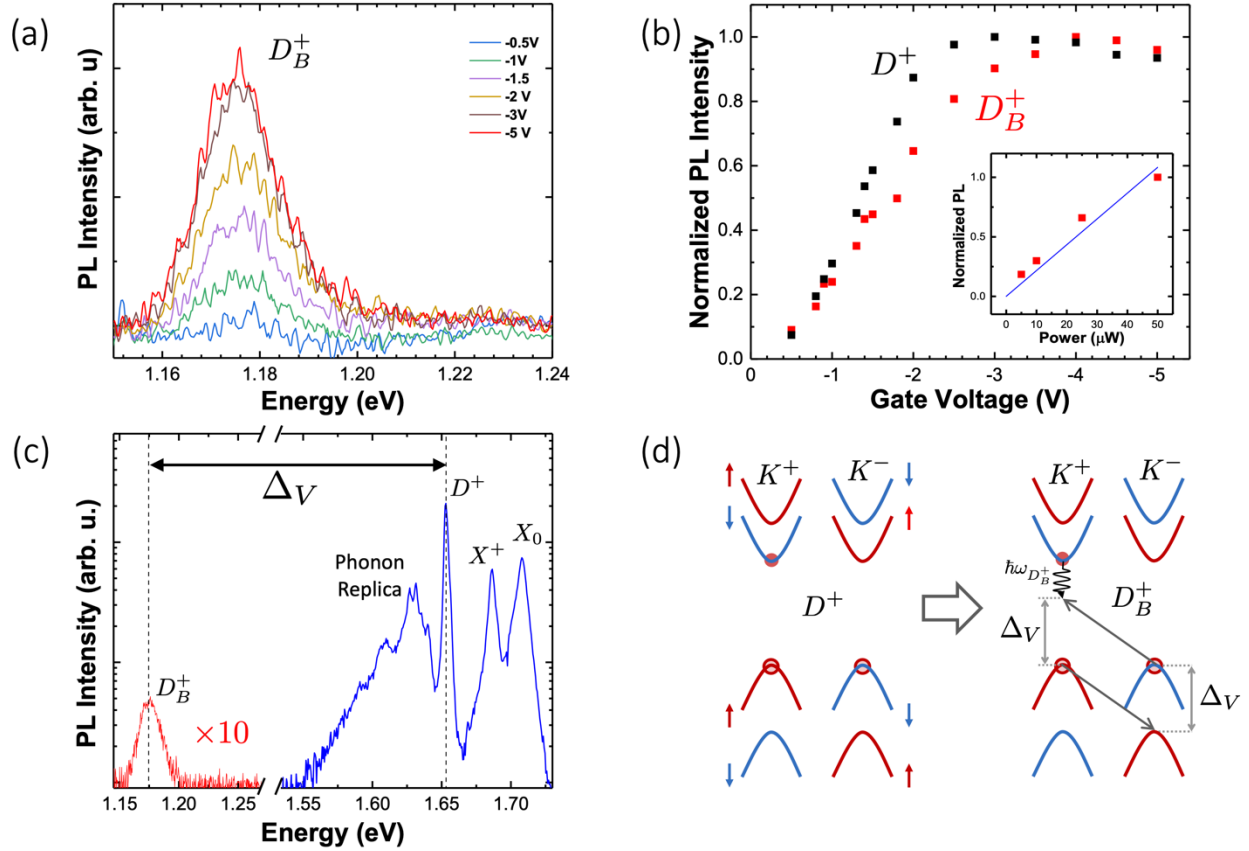


**Fig. 3 Brightened emission of the positively charged dark triion.** **a** PL intensity of the  $D_B^+$  line as a function of the gate voltage; note the energy range which corresponds to emission wavelengths beyond  $1 \mu\text{m}$ . **b** Normalized PL intensity of the dark  $D^+$  and brightened dark  $D_B^+$  triions as a function of the gate voltage; the inset displays the excitation power dependence of the  $D_B^+$  line for a voltage  $V = -5$  volts. **c** Photoluminescence spectrum displayed on a large energy range showing that the energy difference between  $D^+$  and  $D_B^+$  corresponds to the valence band spin-orbit splitting energy:  $\Delta_v = 478 \text{ meV}$ . **d** Schematic of the second order transition corresponding to the radiative emission of the positively charged brightened dark triion  $D_B^+$ . The dark triion  $D^+$  is composed of 2 holes lying in  $K^+$  and  $K^-$  valleys at the top of the valence band (A) and one electron lying at the bottom of the conduction band. The  $D_B^+$  near-infrared recombination results from the hole-hole interaction which allows the radiative recombination of the momentum indirect electron-hole component of the triion. The second hole ends up in the lowest energy valence band (B). The energy difference between the  $D^+$  and  $D_B^+$  lines is simply the valence band spin-orbit splitting  $\Delta_v$  as a consequence of energy and wavevector conservation in the recombination process.

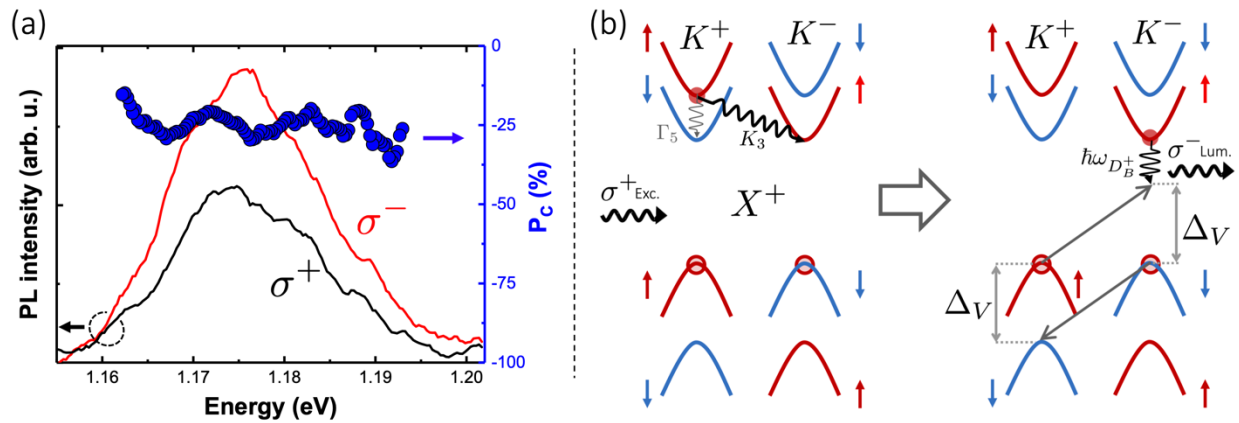


**Fig. 4 Circularly-polarized emission of the positively charged brightened dark trion.** **a** Right ( $\sigma^+$ ) and left ( $\sigma^-$ ) circularly-polarized luminescence of the  $D_B^+$  line following  $\sigma^+$  polarized laser excitation; the corresponding circular polarization  $P_c$  is also displayed (note its negative value). **b** Simplified scheme yielding a negative PL circular polarization of the  $D_B^+$  line as a consequence of the second-order transition (see text).